Full title:

Comparative study between radiofrequency- and muscimol-induced inhibition of cultured networks of cortical neuron

Short title:

Radiofrequency- vs. Muscimol-induced inhibition

Author names:

Clément E. Lemercier[1,2], André Garenne[1], Florence Poulletier de Gannes[1], Corinne El Khoueiry[1], Delia Arnaud-Cormos[3,4], Philippe Levêque[3], Isabelle Lagroye[1,5], Yann Percherancier[1], Noëlle Lewis[1]

Affiliations :

1 Laboratoire de l'Intégration du Matériau au Système, CNRS UMR 5218, University of Bordeaux, Talence, France

2 Faculty of Medicine, Department of Systems Neuroscience, Ruhr University Bochum, Bochum, Germany

3 Univ. Limoges, CNRS, XLIM, UMR 7252, 87000 Limoges, France

4 Institut Universitaire de France (IUF), 75005 Paris, France

5 Paris "*Sciences et Lettres*" Research University, Paris, France

* Corresponding author

E-mail: clement.lemercier@rub.de (CEL)

Abstract

Previous studies have shown that spontaneously active cultured networks of cortical neuron grown planar microelectrode array are sensitive to radiofrequency (RF) fields and exhibit an inhibitory response more pronounced as the exposure time and power increase. To better understand the mechanism behind the observed effects, we aimed at identifying similarities and dissimilarities between the inhibitory effect of RF fields (continuous wave, 1800 MHz) to the γ-Aminobutyric acid type A ($GABA_A$) receptor agonist muscimol (MU). Inhibition of network bursting activity in response to RF exposure became apparent at an SAR level of 28.6 W/kg and co-occurred with an elevation of the culture medium temperature of ~1 °C. Differently to a pharmacological inhibition with MU, exposure to RF fields preferentially inhibits bursting over spiking activity and exerts less constrains on neural network bursting synchrony. Network rebound excitation, a phenomenon relying on intrinsic properties of cortical neurons, was observed consecutively to the removal of tonic hyperpolarization after washout of MU but not in response to cessation of RF exposure which implies that hyperpolarization is not the main driving force mediating the inhibitory effects of RF fields. At the level of single neurons, network inhibition induced by MU and RF fields occurred with reduced action potential (AP) half-width. As change in AP waveform tightly influence efficiency of synaptic transmission, the narrowing effect on AP seen under RF exposure might contribute to reduce network bursting activity. By pointing only to a partial overlap between the inhibitory hallmarks of these two forms of inhibition, our data suggest that the inhibitory mechanisms of action of RF fields differ from the ones mediated by the activation of $GABA_A$ receptor. The rapid onset of the inhibitory effect of RF fields and its reversibility strikingly similar to MU are in favour of a mechanism interacting with fast operating targets at the membrane such as ion channels.

Introduction

Radiofrequencies (RF) are electromagnetic waves ranging from 300 kHz to 300 GHz widely used in modern technology such as telecommunication. The rapid and continuous increase of environmental human-made RF electromagnetic fields (EMF) has raised concerns about their potential risks on health. In particular a large body of research investigated the possible effects of exposure to RF fields used by mobile phones (300-3000 MHz) on the human central nervous system (CNS) (for reviews see van Rongen et al. 2009; Hossmann and Hermann, 2003; Kim et al., 2019). Although it exists evidence pointing to an effect of RF fields on brain oscillations (Croft et al., 2008, 2010, Schmid et al., 2012), evoked potentials (Eulitz et al., 1998; Ferreri et al., 2006, but see Kleinlogel et al., 2008) and glucose metabolism (Volkow et al., 2011) such changes have not been reported to relate to any adverse health effects (ICNIRP 2020; SCENIHR 2015). Interaction between RF and biological systems are best understood on a thermal perspective (Foster and Glasser, 2007; Greenebaum and Barnes, 2019). However, compelling evidence suggest that RF fields may also interact with biological systems by producing so-called non-thermal effects (for reviews see, Belpomme et al., 2018, Hinrikus et al., 2018; Romanenko et al., 2017; although see Apollonio et al., 2013; Foster, 2000 for critical reviews), but so far no mechanisms or molecular targets have been identified. Understanding the biological mechanism of non-thermal effects of RF fields on the CNS is not only critical in promoting safety but also holds the promise of useful insights for the development of future biomedical and biotechnological applications.

Early research on various neural preparation reported electrophysiological change in response to RF fields (Arber, 1981; Arber and Lin 1985; Bolshakov and Alekseev, 1992; Ginsburg et al., 1992; Wachtel et al., 1975). Since then, investigations most frequently indicate that RF fields cause neural activity to decrease (El Khoueiry et al., 2018; Moretti et al., 2013; Pikov et al., 2010; Razavinasab et al., 2016; Romanenko et al., 2014; Saito et al., 2017; Tattersall et al.,

2001; Wang et al., 2017; Xu et al., 2006; but see Bolshakov and Alekseev, 1992; Köhler et al., 2018; Oster et al., 2016; Saito et al., 2018); although the nature of the observed effects might depends on the RF frequency bands at which neural preparation is exposed (for example see El Khoueiry et al., 2018 vs. Saito et al., 2018). In the recent years, our lab developed an experimental setup allowing to simultaneously record and expose to RF fields spontaneously active cultures of cortical neurons grown on a planar microelectrode array (MEA) (Merla et al., 2011). Results obtained with this system indicate that networks bursting activity decrease when exposed to RF fields (Moretti et al., 2013) and that the inhibitory response is function of exposure time and power (El Khoueiry et al., 2018). Experiments done with equivalent thermal heating suggested that the inhibitory effects of RF fields may originate in part from non-thermal interaction with the nervous tissues. However, the mechanism of action of RF fields on neural networks remained elusive.

In the present study, we aimed to contribute to the understanding of the mechanisms of action behind the inhibitory effects of RF fields on cultured cortical neural networks by performing a direct comparison with the inhibitory effects of the $GABA_A$ receptor agonist, muscimol (MU). The $GABA_A$ receptor is the major inhibitory neurotransmitter receptor responsible for fast inhibition in the mammalian brain (Olsen and Sieghart 2008; Sallard et al., 2021). Signaling at this receptor is well understood thus making it a solid reference for comparative studies aiming to infer potential mechanisms of actions of particular drugs or treatments. Experiments were carried on a new MEA device with improved stability during EMF exposure (Nefzi et al., 2022) and changes in spiking, bursting activity and action potential (AP) waveform in response to RF fields or MU were analyzed and compared. This comparative approach allowed us to identify similarities and dissimilarities between these two forms of inhibition and to employ them as a basis for unravelling a potential mechanism of action of the inhibitory effect of RF fields on cultured neural networks.

Materials and methods

Animals

Primary cultures of neocortical neuron were prepared from embryos of gestating Sprague-Dawley rat (Charles River Laboratories, L'Arbresle, France). Experiments involved six gestating rats. All procedures were carried out incompliance with the European Community Council Directive for the Care and Use of laboratory animals (2010/63/EU) and protocols were approved by the Ethics Committee for Animal Care and Experimentation CEEA 50 of Bordeaux.

Preparation of primary neural culture

Preparation of primary neural cultures was identical to the methods described in El Khoueiry et al., (2018) and Moretti et al., (2013). In brief, under anaesthesia (5% isoflurane), gestating rats were euthanized by cervical dislocation, embryos (at embryonic day 18) were collected, and their cortices were dissected and treated with a papain-based dissociation system (Worthington Biochemical, Lakewood, CO). Following mechanical dissociation and two steps of centrifugation (the second with an albumin-inhibitor solution), the pellet containing cortical cells (glial cells and neurons) was resuspended in a neurobasal culture medium (NBM) supplemented with 2% B-27, 1% GlutaMAX, and 1% penicillin-streptomycin (Fisher Scientific, Illkirch, France). The recording chips of autoclaved MEAs (Multi Channel Systems MCS, Reutlingen, Germany) previously coated with polylysine and laminin (Sigma-Aldrich, St. Quentin-Fallavier, France) were plated with a drop of cellular suspension containing 10^5 cells. Cells were left to sediment and adhere on the MEA chip for up to 2 h and MEA chambers were then filled with 1 mL of NBM. MEAs were kept in individual petri dish at 37°C in a humidified incubator with 5% CO_2 until mature neural network development. Culture medium were half-exchanged every 48 h until recordings.

New MEA design and characteristics

In the present study, a modified version of a 60-channel planar MEA introduced in Merla et al., (2011) was used. This new design shared the main characteristic of these MEAs namely the amplifier contact pads placed underneath the printed circuit board but presented as main evolutions a reduced chip aperture to the limits of the recording zone and several ground planes in the multi-layered PCB. These evolutions allowed this device to be steadier in terms of Specific Absoption Rate (SAR) and temperature stability during EMF exposure (see Nefzi et al., 2022, for numerical and experimental dosimetry of the device). In this modified MEA, SAR values normalized per 1 Watt of incident power was estimated at 5.5 ± 2.3 W/kg.

Electrophysiology and exposure system

The experimental setup for simultaneous electrophysiological recordings and exposure to RF or pharmacological agents comprised a MEA coupled to an open transverse electromagnetic cell (TEM) (Merla et al., 2011, Soueid et al. 2014, Nefzi et al., 2022) and a perfusion system allowing continuous fresh medium exchange with minimal disturbances. RF CW signal at 1800 MHz was delivered to the open TEM cell with a signal generator-amplifier (RFPA, Artigues-près-Bordeaux, France). Different incident powers were delivered by the generator up to 6.9 W resulting in SAR levels comprised between ~4.8 and ~37.9 W/kg. Heating of the culture medium in response to RF exposure at different SAR levels was measured with a fiber optic probe (Luxtron One, Lumasense Technologies, CA, USA, ± uncertainty 0.1°C) immersed in the culture medium.

To enable simultaneous recording and exposure to RF fields, MEAs were maintained “sandwiched“ between the TEM bottom plate and the preamplifier (MEA1060-Inv, Multi-Channel

Systems, MCS, Reutlingen, Germany), as described in previous publications (El Khoueiry et al., 2018; Merla et al., 2011; Moretti et al., 2013; Nefzi et al., 2022). Once installed on the MEA amplifier, a perfusion holder (MEA-MEM-PL5, ALA Scientific Instruments Inc. USA) was inserted into the MEA chamber. Perfusion of fresh culture medium was controlled with a peristaltic pump (REGLO ICC, Hugo Sachs Elektronik, Germany) and optimal perfusion rate (causing minimal disturbances to neural cultures) was set at ~350 µL/min. In these conditions, culture medium was fully exchanged in ~2:50 min. Prior to starting of the experiment, cultures were let to acclimate to continuous medium exchange for ~30 min. Recordings were performed in a dry incubator at 37 °C with 5% CO_2. Preamplification gain was 1200 and signals were acquired and digitized at 10 kHz/channel with an MCS-dedicated data acquisition board (MC_Card, MCS). Signals were recorded and visualized with the software MC Rack (MCS). After 30 min of baseline recording, neural cultures were exposed for 15 min either to a sham treatment (SH), a pure continuous carrier radiofrequency (RF, CW) at 1800 MHz, or to the $GABA_A$ receptor agonist muscimol (MU), (Tocris Bioscience, Bristol, UK). After treatment, post-treatment activity was continuously monitored for 45 min. Data from culture aged of 17 to 27 days in vitro (DIV) were included in the present study (DIV, Median = 20, Interquartile range, IQR = 4.5, n = 35, all experimental groups collapsed).

Data analysis and metrics

Processing and analysis of multi-channel data was performed with the software package SPYCODE (Bologna et al., 2010) developed in MATLAB environment (Mathworks, USA). After signal filtering (Butterworth high-pass filter with a cut-off frequency at 70 Hz), spike detection was performed with the differential threshold precision timing spike detection (PTSD) method described by Maccione et al., (2009) and spike trains were analysed for bursts detection using the method described by Pasquale et al., (2010). Change in neural networks activity in

response to 15 min of SH, RF or MU exposure was assessed at the level of the entire MEA by pooling data from all active channels (i.e. showing both spiking and bursting activities). Burst detection was used to compute the mean bursting rate (MBR), mean interburst interval (IBI), mean burst duration (BD), mean intraburst spike rate (IBSR) and crossed analysis between burst periods and spike trains allowed to compute the mean spiking rate (MSR) for spikes occurring outside bursts. Effects of RF and MU exposure were compared in respect to the SH group after data normalization reflecting the average fractional variation (*R*) of a metric (*M*) during the exposure phase ($M_{Exposure}$) relative to the baseline reference phase ($M_{Baseline}$).

$$R_M = M_{Exposure}/M_{Baseline}$$

Level of synchronicity for descriptors of bursting activity across MEA's channels was evaluated with the coefficient of variation (CV) defined as the ratio (expressed in %) of the average channels standard deviation to the metric mean value (either IBI, BD or IBSR). The lower the CV, the higher synchronization across MEA's channels (Bader et al., 2017; Baltz et al., 2010). Inter-channels variation for MBR and MSR relative to the overall average fractional variation (i.e. entire MEA) was used to describe the spatial variability of the effects associated to treatment. This measure was evaluated by computing the normalized root mean square error (*Norm. RMSE*) as follow:

$$Norm.RMSE = \frac{\sqrt{\sum_{k=1}^{K}(Y - y_k)^2}}{K \cdot Y}$$

Where *'Y'* is the averaged normalized value of MBR or MSR over all MEA's channels (*K*) and '*y'* is the averaged normalized value of MBR or MSR at the level of individual channels (*k*). For example, a *Norm. RMSE* value equal to 0.5 indicates that the mean inter-channels variation to the mean is of 50 %. Computation methods for the metrics described above are reported in S1 table.

AP sorting and waveform analysis

AP detection and sorting was performed with the software Offline Sorter V3 (Plexon Inc, TX, USA) over a period of 30 min including 15 min of baseline (pre-exposure phase right prior to treatment) and 15 min when neural cultures are continuously exposed to the treatment. To ensure reliable sorting between the two recording phases, pre-exposure and exposure phases were merged into a single file with the software MC_dataTool (MultiChannel Systems, Germany). Detection threshold was set at five times the standard deviation of the channel noise level and waveform sample wide containing single event was set at 4 ms (40 sample, 0.8 ms before peak and 3.2 ms after peak). Note that this method of detection differs from the one used in SPYCODE. AP sorting was performed using the T-Dist E-M method (Outlier Threshold 1.5; D.O.F. Mult. 8) and analyses were executed in batch mode. This method allowed to detect in average 67 991 ± 10 655 (Mean ± SEM) APs per MEA and to sort in average 40 135 ± 6 114 APs per MEA (S1A Fig, data over 15 min during pre-exposure phase from 15 cultures of the RF group used here as representative). Unsorted APs were not analyzed. Hierarchical clustering of the sorted APs indicated that MEA's channels presented several sources of AP that were qualified either as major (MAJ), auxiliary (AUX) and minor (MIN) contributors of the total number of sorted spike (S1A and S1B Fig). In average, MAJ, AUX and MIN AP clusters were respectively observed in 85.3 ± 3.6, 28 ± 4.5, 12.3 ± 1.8 % of the MEA's channels and enclosed respectively in average 68 ± 4.4, 21.4 ± 2.5, 10.6 ± 3.3 % of the total amount of sorted AP (S1A Fig). Crossing of AP timestamps with the burst periods indicated for the MAJ AP cluster that sorted APs inside bursts ($_{AP}$IB) were around two times more numerous (~1.9) than sorted AP outside bursts ($_{AP}$OB) and that this proportion decreased to ~1.3 and ~1.1 respectively for the AUX and MIN AP clusters (S1A Fig). As ~89% of the total amount of sorted APs were en-

closed in the MAJ and AUX AP clusters, only waveforms from these two clusters were analysed. From these waveforms, peak, anti-peak amplitude, full width at half maximum (FWHM, through linear interpolation), maximal as slope of the rising edge and falling edge were measured. Data from MAJ and AUX cluster were then averaged to reflect the overall change in AP waveform in response to treatments. Metrics used to quantify change in AP waveforms are illustrated in S1C fig and defined in S3 Table.

Statistics

Statistical analysis was performed using the software R (R Core Team 2021) and the 'PMCMRplus' library (Pohlert 2020). Unless stated, data in text and supporting information are reported as median and interquartile range (IQR, .i.e. the differences between Q3 and Q1). To evaluate changes relative to baseline, raw values at baseline for the different metrics showed in Figs 2 and 5 are reported respectively in tabulated form in S2 and S4 Table. A Kruskal-Wallis test followed by a Conover's multiple comparison test was used to compare differences between groups. A p-value < 0.05 was considered statistically significant. Effect size (epsilon-squared, ε^2), when reported, was calculated with the "rcompanion" (Mangiafico, 2020) R package. Data were plotted with the 'ggplot2' (Wickham, 2016) and 'ggpubr' (Kassambara, 2020) R packages. The compact letter representation method (Piepho, 2004) was used to denote statistical significance after pairwise comparisons with the R package 'multcompView' (Graves et al., 2019). Pairwise comparisons sharing a common letter are not statistically different and, on the contrary the ones not sharing any letter are statistically different.

Results

Dose response relationship of RF- and MU-induced inhibition.

A photography of the setup illustrating the different parts is shown in Fig 1A. Heating of the culture medium increase with SAR level (Fig 1B). After 15 min of exposure, heating peaks ranged from ~0.2 to ~1.5°C respectively for minimal (~4.8 W/kg) and maximal (~37.9 W/kg) tested SAR levels. As cultured networks of cortical neuron are sensitive to RF fields in a dose dependent manner (El Khoueiry et al., 2018), the response relationship between MBR and exposure levels was re-evaluated for the new MEA device used in the present study. With this new type of MEA, inhibition of bursting activity became visible for exposure levels over ~25 W/kg and a reduction of ~50 % in MBR was estimated at ~28.6 W/kg (Fig 1C). At this SAR level, reduction of bursting activity after 15 min of exposure co-occurred with an elevation of the medium temperature of ~1 °C. To compare the effects of RF exposure with those of the $GABA_A$ receptor agonist MU under similar level of inhibition, the relation between MBR and MU concentration was firstly evaluated (Fig 1D). MU exerts a profound inhibitory action on the activity of cultured cortical networks and its half maximal inhibitory concentration for the metric MBR ($IC_{50\text{-}MBR}$) was estimated to ~0.25 µM, a value in accordance with other studies on basic receptor and neural cultures pharmacology (Bader et al., 2017; Dunn and Thuynsma, 1994; Novellino et al., 2011; Rijal and Gross, 2008).

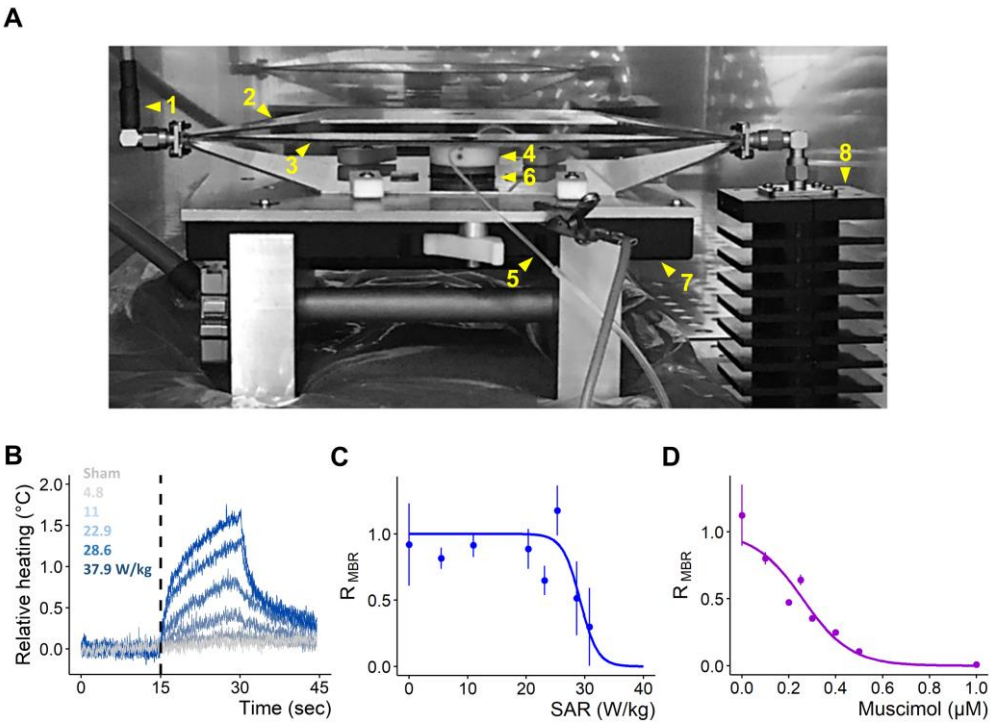

Fig 1. Setup configuration and dose response profile of MBR against SAR level and MU concentration. (A) Photography of the setup configuration used for simultaneous recording on MEA and exposure to RF and pharmacological agents. (1) Coaxial cable connecting an RF-generator/amplifier (located outside the incubator) to (2) an open transverse electromagnetic (TEM) cell. (3) TEM cell septum. (4) Perfusion holder inserted on top of the MEA chamber. (5) Perfusion microtubes for medium exchange. (6) MEA "sandwiched" between TEM bottom ground plate and amplifier ground plate. (7) Inverted MEA preamplifier connected to a MC_Card of a desktop computer. (8) 50 Ω Terminator. (B) Relative heating response of the culture medium over 15 min in function of different SAR level (W/kg). (C) Dose-response relation between SAR and MBR; results from 21 recordings (18 cultures), 0 (W/kg): n = 21; 5.5: n = 2; 11: n = 3; 20.35: n = 2; 23.1: n = 3; 25.3: n = 3; 28.6: n = 5; 30.6: n = 3. (D) Dose-response relation between MU concentration and MBR; results from 14 recordings (3 cultures), $1e^{-4}$ (µM): n = 2; 0.1: n = 3; 0.2: n = 1; 0.25: n = 2; 0.3: n = 1; 0.4: n = 1; 0.5: n = 2; 1: n = 2. (C-D) Normalized MBR, ratio of the exposure phase to baseline, data shown as Median ± SD. Fits computed with non-linear least squares method, Pearson's Goodness-of-Fit: $p < 0.05$.

RF and MU differentially impacted network activity patterns

The inhibitory effects of RF and MU were then compared in respect to an SH group after data normalization (see materials and methods). Definitions of the metrics used to describe change in network activity in Fig 2 are reported in S1 Table. To assess the magnitude of the reported normalized effects in respect to the raw data, raw data at baseline relative to Fig 2 are tabulated in S2 Table.

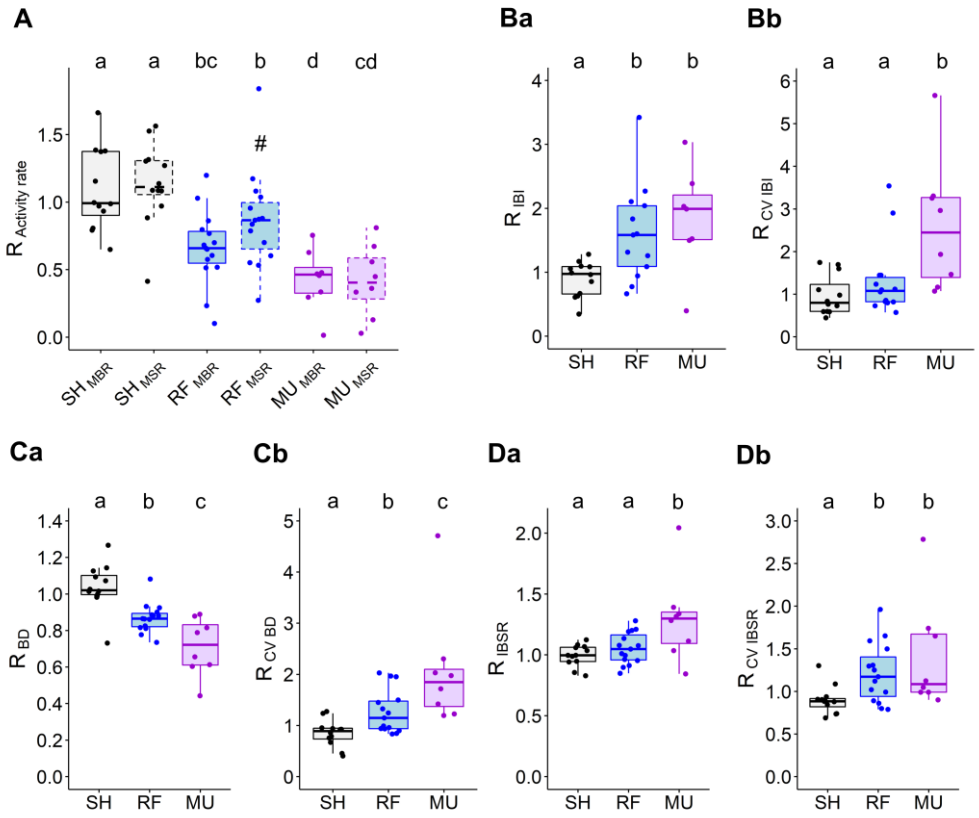

Fig 2. Comparison between RF and MU-induced inhibition of cultured cortical network. (A) Average effect of 15 min of exposure to RF and MU on MBR and MSR (spike outside burst periods). Boxplots with dashed box denote MSR data."#" is indicative of p = 0.0535 against RF_{-MBR} and RF_{-MSR}. (Ba) Average effect of 15 min of exposure to RF and MU on mean inter-burst interval (IBI), (Ca) mean burst duration (BD), (Da) mean inter-burst spike rate (IBSR). (Bb, Cb and Db) Coefficients of variation (CV) respectively for IBI, BD and IBSR. Normalized data, ratio of the exposure phase to baseline. SH: n = 12; RF: n = 15; MU: n = 8.

Exposure to RF (SAR of 28.6 W/kg) or MU (0.25 µM) both reduced MBR (RF: ~35% reduction, SH/RF, $p < 0.001$; MU: ~57% reduction, SH/MU, $p < 0.001$) and MSR (RF: ~14% reduction, SH/RF, $p < 0.001$; MU: ~58% reduction, SH/MU, $p < 0.001$). Inhibitory effect of MU on bursting and spiking activities were on average stronger than for RF exposure (RF_{-MBR}/MU_{-MBR}, $p = 0.0412$; RF_{-MSR}/MU_{-MSR}, $p < 0.001$, - Fig 2A). In comparison to MU, RF showed a tendency to preferentially inhibits bursting over spiking activity whereas MU reduced equivalently both type of activity (RF_{-MBR}/RF_{-MSR}, $p = 0.0543$, $\varepsilon^2_{RF\text{-}MBR} = 0.387$, $\varepsilon^2_{RF\text{-}MSR} = 0.267$; MU_{-MBR}/ MU_{-MSR}, $p = 0.9057$, $\varepsilon^2_{MU\text{-}MBR} = 0.692$, $\varepsilon^2_{MU\text{-}MSR} = 0.607$).

Inhibition of neural networks activity was evaluated in the spatial domain by quantifying the inter-channel variability of MBR and MSR variations across all channels of the MEA layout by computing the normalized root mean square error (Norm. RMSE, see materials and methods). Intrinsic variation of this measure observed in response to SH exposure indicated in average that the level of spatial variability for MBR was slightly lower than for MSR (SH_{-MBR} = 0.22 (0.14); SH_{-MSR} = 0.37 (0.30); p = 0.0327). This observation suggests that spiking activity fluctuated more over the MEA space whereas bursting activity was more synchronized in space. RF- and MU-induced inhibition were both associated to a comparable level of spatial variation of bursting activity across the MEA's channels (RF = 0.20 (0.22); MU = 0.28 (0.12); p = 0.3059). The degree of spatial variability in MBR was not different from the intrinsic spatial variability observed in response to SH exposure (p = 0.3024). Similarly to MBR, data for MSR indicated that RF- and MU-induced inhibition caused spiking activity to variate equivalently in space (RF = 0.54 (0.16); MU = 0.65 (0.21); p = 0.1848) but spatial fluctuations of MSR were higher than for the intrinsic variation observed in SH exposure (p = 0.0037, pooled MSR data across RF and MU); although as in SH exposure, spatial variations of MBR were lower than for MSR (p < 0.001). Collectively these data indicate that RF-induced inhibition occurred within the MEA space as diffusely as the pharmacological inhibition induced by MU.

Comparison between RF- and MU-induced inhibition was pursued with descriptors of bursting activity such as IBI, BD and IBSR and their respective indicators of synchronicity across MEA's channels with the coefficient of variation (CV, see materials and methods and metrics definition in S1 Table). In response to RF and MU, bursting activity become sparser as seen by increased IBI (SH/RF, p = 0.0020, SH/MU, p < 0.001; RF/MU, p = 0.4528 - Fig 2Ba). In opposition to RF exposure, the inhibitory action of MU was accompanied with a desynchronization of bursting activity across MEA's channels as seen by increased CV IBI (SH/RF, p = 0.2318; SH/MU, p < 0.001; RF/MU , p = 0.0098 - Fig 2Bb). RF and MU both decreased BD

(SH/RF, $p < 0.001$; SH/MU, $p < 0.001$; RF/MU, $p = 0.0178$ - Fig 2Ca) and desynchronized BD across MEA's channels (CV BD: SH/RF, $p = 0.0035$, SH/MU, $p < 0.001$ - Fig 2Cb) but this effect was of higher magnitude for MU (RF/MU , $p = 0.0128$). MU, but not RF exposure, increased IBSR (SH/RF, $p = 0.2919$; SH/MU, $p = 0.0069$; RF/MU, $p = 0.0476$ - Fig 2Da). However, both treatments desynchronized IBSR across MEA's channels (CV IBSR: SH/RF, $p = 0.0062$; SH/MU, $p = 0.0042$; RF/MU, $p = 0.5388$ - Fig 2Db). Results obtained on the alteration of descriptors of bursting activity and synchronicity in response to MU corroborate with previous investigations under similar experimental conditions (Bader et al., 2017).

Differential effect of RF and MU on neural networks temporal activity pattern

Analysis and comparison of the two forms of inhibition was pursued in the temporal domain by measuring bursting rate (BR) and spiking rate (SR) over time (Fig 3). In response to RF or MU, BR dramatically decreased by about half of the baseline level within the minute following exposure onset (Fig 3A). Similarly to BR, SR reduced within the minute following exposure onset but in contrary to MU the later appeared in average to be less affected by RF (Fig 3B). Quantification of the rate of BR inhibition during the initial phase of exposure (initial inhibitory rate, see metrics definition in S1 Table) indicated that RF and MU both impacted BR with an equivalent initial potency (SH/RF, $p < 0.001$; SH/MU, $p = 0.0035$; RF/MU, $p = 0.9243$ - Fig 3C). Initial inhibitory rate for SR in response to RF showed a greater level of variability than for BR and was not different to SH (SH/RF, $p = 0.1741$ - Fig 3C). On the other side, MU inhibited BR and SR with an equivalent initial potency (SH-$_{SR}$/MU-$_{SR}$, $p < 0.001$; MU-$_{BR}$/MU-$_{SR}$, $p = 0.6850$ - Fig 3C). Following the initial action of the treatments, BR and SR showed a tendency for a slight regain of activity, although this effect was more marked for MU.

In response to washout of MU, a dramatic short-lasting regain of activity of about 1 min was observed. This phenomenon qualified as postinhibitory rebound (PIR, see metrics definition in

S1 Table) was in average visible both for BR and SR (Fig 3A and 3B) but only significantly detected for bursting activity (SH-$_{PIR-BR}$/ MU-$_{PIR-BR}$, p = 0.0128; SH-$_{PIR-SR}$ / MU-$_{PIR-SR}$, p = 0.0549 - Fig 3D). Interestingly, PIR was not observed in response to RF exposure cessation (SH-$_{PIR-BR}$ / RF-$_{PIR-BR}$, p = 0.8420; SH-$_{PIR-SR}$ / RF-$_{PIR-SR}$, p = 0.9821 - Fig 3D). Successive recording phases indicated that neuronal networks activity fully recovered from treatments and temporally evolved similarly to SH.

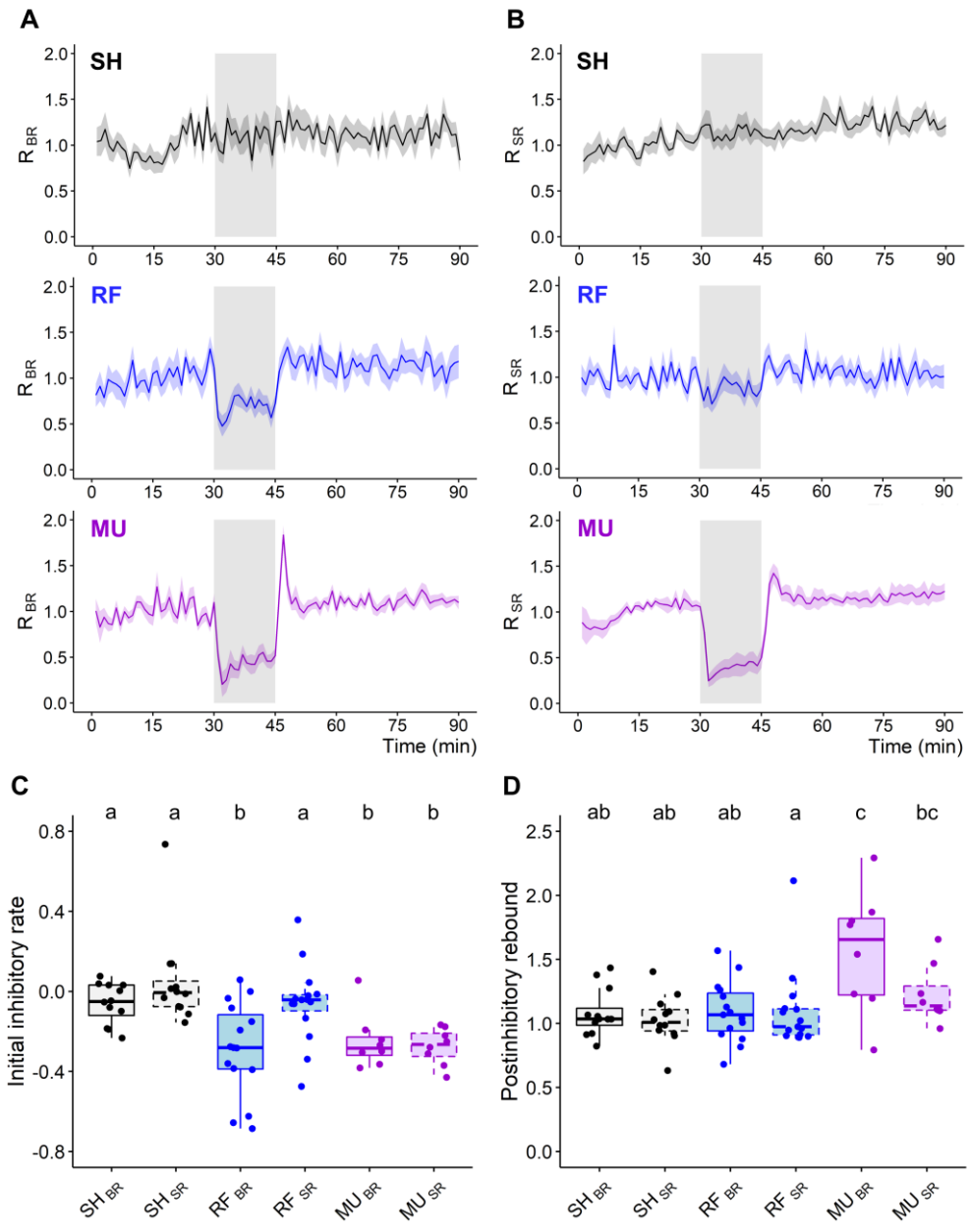

Fig 3. Temporal dynamic of RF and MU-induced inhibition on bursting and spiking rates. (A-B) Normalized temporal time course of bursting rate (BR, left) and spiking rate (SR, right) over 90 min for SH (top), RF (middle) and MU (bottom) groups (1 min bin-size, data show as Mean ± SEM). The exposure phase is symbolised by a grey shadowed area. (C) Initial inhibitory rate in response to RF and MU exposure. (D) Quantification of postinhibitory rebound in response to treatment cessation. Boxplots with dashed box denote SR data. SH, n = 12; RF, n = 15; MU, n = 8.

Similarities and dissimilarities in the temporal domain between the two treatments are once more exemplified in Fig 4A and 4B with data from two representative cultures exposed either to RF or MU. In these examples, the MU experiment is initially marked by an abrupt shutdown

of neural activity lasting a few minutes followed by a slight and gradual replenishment of activity. Following washout of MU, network BR undergoes a short period of rebound excitation which next re-stabilize (note the absence of rebound excitation for SR). On the contrary, the RF exposure experiment did not display such dynamics but was rather associated with a strict slow-down of network activity with bursts peaking less frequently above the normalization line.

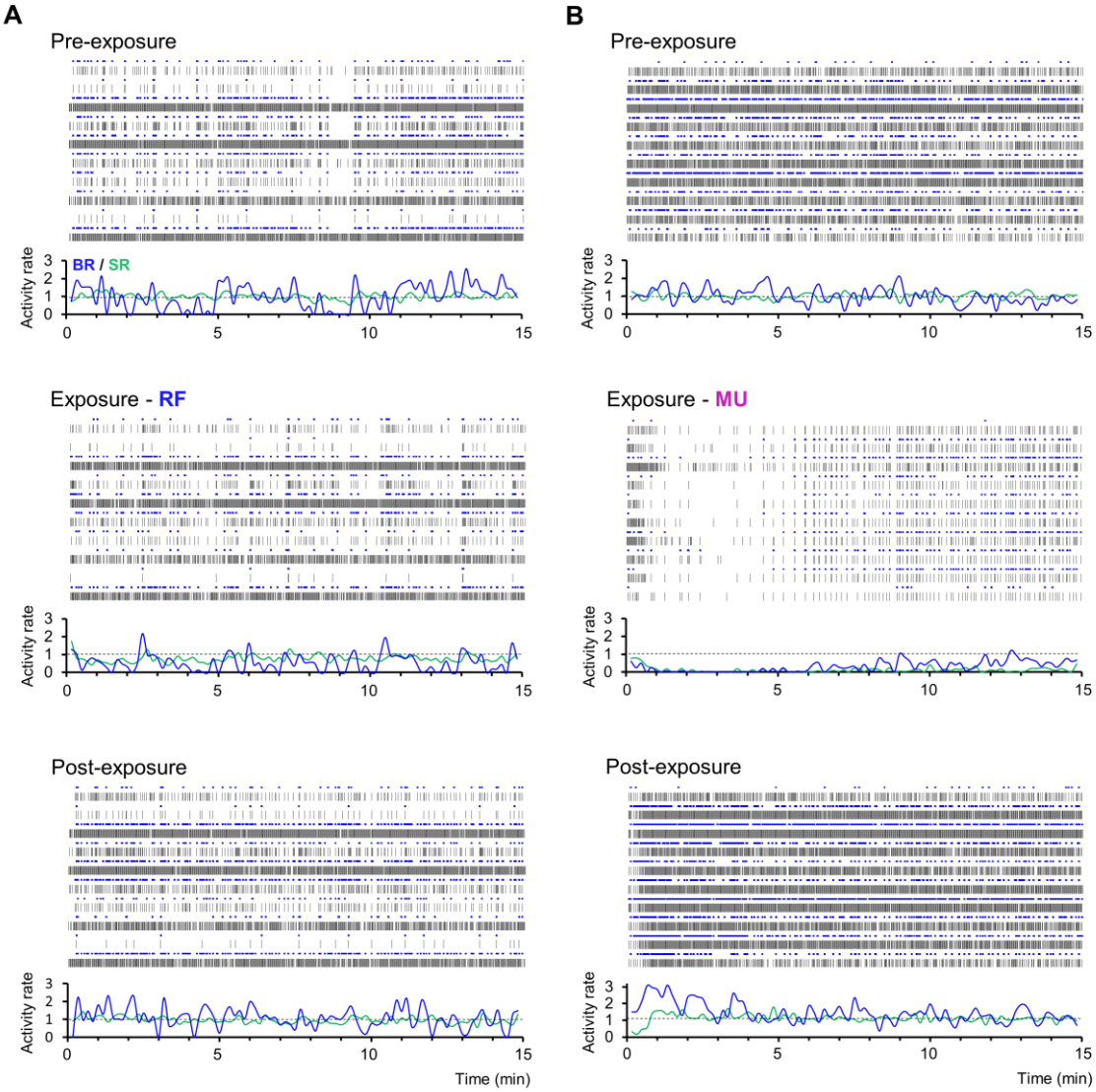

Fig 4. Representative recordings showing the temporal time course of RF- and MU-induced inhibition of neural networks. (A-B) Data from 10-selected electrodes of 2 independent cultures either exposed to RF (left) or MU (right) showing spiking (SR) and bursting rate (BR) along three recording segments of 15 min during pre-exposure (top), exposure (middle), and post-exposure recording phases (bottom). Neural activity is shown as spike raster plot caped in blue for markers of burst detection. Below each raster plot is the corresponding normalized BR (blue) and SR (green) computed overtime along non-overlapping sliding windows of 10 sec, dashed lines represent the normalization level.

RF and MU similarly alter AP waveform

The inhibitory effects of RF and MU were next analysed and compared at the level of single-unit activity by evaluating change in APs waveform (Fig. 5). Definitions of the metrics used to describe change in AP waveform are illustrated in S1C fig and defined in S3 Table. To assess the magnitude of the reported normalized effects in respect to the raw data, raw data at baseline relative to Fig 5 are tabulated in S4 Table. After hierarchical clustering of spike events, data from the two main AP clusters were analysed in a pooled manner (see materials and methods section and S1 Fig. for more details on AP detection, sorting, cluster repartition and waveform analysis).

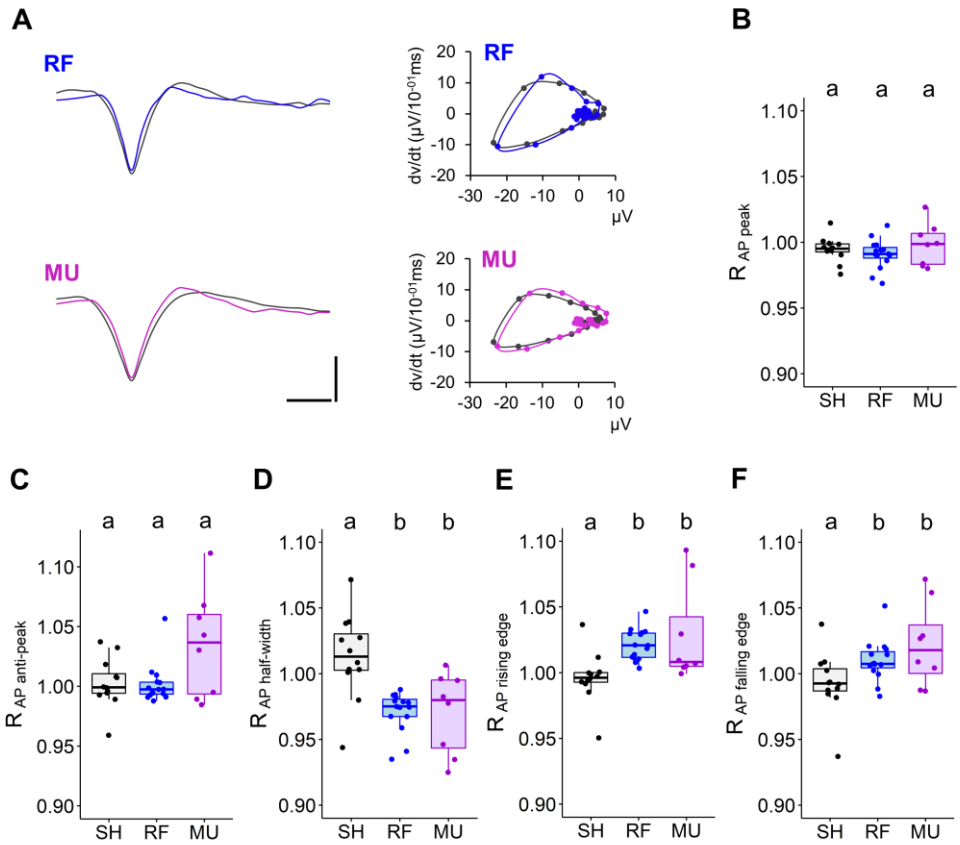

Fig 5. Change in AP waveform in response to RF and MU exposure. (A) Representative average AP traces from a single unit (left) and associated phase plot (right) before and during exposure to RF (top) and MU (bottom). Scale: (y): 15 µV; (x): 500 µs. (B-F) Boxplots showing variation in AP peak (B) and anti-peak amplitude (C) half-width (D) maximal rising (E) and falling edge (F). Normalized data, ratio of the exposure phase to baseline. SH, n = 12; RF, n = 15; MU, n = 8.

The average effects on AP waveform in response to RF and MU are shown from two representative single units and their respective phase plots in Fig 5A. Analysis of AP waveforms indicated in respect to SH that RF and MU exposure neither impacted AP peak amplitude (p = 0.3511 - Fig 5B) or anti-peak amplitude (p = 0.2859 - Fig 5C), but that both treatments narrowed AP half-width (SH/RF, $p < 0.001$; SH/MU, p = 0.0018; RF/MU, p = 0.6065 - Fig 5D). This narrowing effect occurred symmetrically with both depolarisation and repolarisation phases occurring at faster rate (slope of the rising edge: SH/RF, $p < 0.001$; SH/MU, p = 0.0038; RF/MU, p = 0.3547 - Fig 5E; slope of the falling edge: SH/RF, p = 0.0374 ; SH/MU, p = 0.0224; RF/MU, p = 0.5659 - Fig 5F). In agreement, phase plot shows generally, albeit of small amplitude, steeper slopes along the AP cycle. Analysis of effect size indicated stronger effect size on the rising than on the falling edge of the AP (RF: $\varepsilon^2_{rising} = 0.475$; $\varepsilon^2_{falling} = 0.194$; MU: $\varepsilon^2_{rising} = 0.384$; $\varepsilon^2_{falling} = 0.180$) suggesting that narrowing of the AP half-width in response to RF and MU occurred primarily through a mechanism that increases the depolarisation slope.

Discussion

In the present study, exposures to RF fields were performed at a SAR level of 28.6 W/kg, a value ~1.4 times lower than levels used in El Khoueiry et al., (2018) and Moretti et al., (2013). Indeed a recent re-evaluation of the dosimetry (Nefzi et al., 2022) indicated estimated SAR values per Watt of incident power of 5.5 ± 2.3 W/kg and 40.3 ± 5.3 W/kg respectively for the present and former MEA version (El Khoueiry et al., 2018 and Moretti et al., 2013). This re-evaluation was made possible thanks to the continuous progress in experimental and numerical dosimetry and better assessment of influencing environmental factors (Nefzi et al., 2022). The SAR level of 28.6 W/kg is however higher than local basic safety restriction fixed at 2.0 W/kg (ICNIRP, 2020). Therefore this study is rather limited regarding potential adverse effects of human-made environmental RF fields on health. Exposition to RF for 15 min at a SAR level of

28.6 W/kg decreased reversibly bursting activity of ~35 % and co-occurred with an elevation of the culture medium temperature of ~1 °C. Activity rate of neural culture is influenced by temperature with hypo- and hyperthermia being respectively associated to lowered and heightened neural activity (El Khoueiry et al., 2018; Köhler et al., 2018; Rubinsky et al., 2007; Wang et al., 2011; but see Zwartsen et al., 2020). In line with data reported in these studies, previous experiments from our lab showed that heating of the culture medium of ~1°C slightly increased bursting activity (El Khoueiry et al., 2018) thus suggesting that the observed effect of RF fields might have in part non-thermal origins.

We previously reported that exposure to RF fields decrease bursting activity of cultured networks of cortical neuron (Moretti et al., 2013) and that this inhibitory effect increases as exposure time and SAR level increase (El Khoueiry et al., 2018). In the present study, investigations of the inhibitory effects of RF fields were pursued by performing a direct comparison with the effects of the $GABA_A$ receptor agonist MU. Our results showed that in contrast to MU, RF preferentially inhibits bursting over spiking activity. Although spiking activity was reduced by RF exposure, inhibition was more variable and weaker than for bursting activity. Other studies with cultured networks of cortical neuron also reported that MU equivalently inhibits spiking and bursting activity (Bader et al., 2017; Novellino et al., 2011). GABAergic inhibition in the brain can be classified as either phasic or tonic (Farrant and Nusser, 2005). The first depends on fast activation of synaptic $GABA_A$ receptors from synaptically released GABA whereas the second depends on sustained activation of peri- and extrasynaptic $GABA_A$ receptors by ambient GABA. In our experiments, continuous application of MU in the culture medium activates both synaptic and peri-extrasynaptic $GABA_A$ receptors which ultimately leads to a tonic neural hyperpolarization. Neuronal excitability is in essence equivalently reduced throughout the network subcomponents and an equivalent reduction in activity patterns based on regular spiking, intrinsically busting neurons as well on network collective bursting behavior is observed. As

RF exposure differentially impacted spiking and bursting activity, one may argue that cell hyperpolarization is not the main force driving the inhibitory effects RF on neural networks. Studies on the effect of RF on the membrane potential of excitable cells (cardiomyocytes and neurons) has led to conflicting results, with some showing no effect (Arber and Lin 1985; Linz et al., 1999; Marchionni et al., 2006; Wachtel et al., 1975), hyperpolarization (Romanenko et al., 2014), or both depending on the studied region after whole animal acute exposure (Wang et al., 2017). Detailed electrophysiological investigations in our experimental conditions are needed to shed light on this point.

At cellular level, cortical neurons can generate bursts based on intrinsic properties such as hyperpolarization-activated current (I_h), subthreshold membrane oscillations and T-type calcium current above which high frequency action potentials fire for a brief period (Cain and Snutch, 2013; Perez-Reyes, 2003; Wu et al., 2001). At network level, bursts can be generated intermittently in a collective manner as an emergent property (van Pelt et al., 2004; Wagenaar et al., 2006) relying on the development of an excitatory-inhibitory oscillating network (Fardet et al., 2018, Teppola et al., 2019). On these perspectives, hypothesises could be that reduced bursting activity in response to RF is due to a predominant action on intrinsically bursting neurons over regular spiking neurons, or alternatively that the effect of RF manifest on larger scale by reducing network collective bursting behavior. Interestingly, some authors suggested that the extremely low-frequency EMFs (high-intensity power frequency, 50 Hz) enhance the activity of cultured networks of cortical neuron by modulating the activity of pacemaker-like interneurons (Saito et al., 2018). At our knowledge, this research avenue has not been yet further investigated by other laboratories. Nevertheless, our experiments focused on mature neocortical cultures where network bursts substantially contribute to the overall burst count (~60 to ~80% of the total number of bursts) and no discrimination in our analysis was applied between isolated bursts and network bursts. Therefore, the observed inhibition of bursting activity in response to

RF exposure mostly originates from a reduction of network collective bursting behavior. Exposure to RF at different level of culture maturity (i.e. irregular and slightly synchronized bursting vs. regular and highly synchronized bursting) is of interest to determine whether neural network topology is a factor determining the sensitivity to RF. Moreover, detailed analysis with improved detection algorithms could help to better tease apart the effect of RF on the different network subcomponents and related activity patterns.

Descriptors of neural networks bursting activity were similarly impacted by RF and MU exposure. In the two forms of inhibition, decreased MBR was accompanied by increased IBI and decreased BD, but data suggested that only inhibition induced by MU was accompanied by increased IBSR. However, the reported effect of MU on IBSR is in opposition with a recent thorough study done under similar experimental condition (Bader et al., 2017), thus making difficult to test the pertinency of this observation in comparison to RF. At neural networks level, shift in the balance between excitation and inhibition strongly contribute to control burst phase, termination and intraburst spiking rate (Arnold et al., 2005; Bader et al., 2017; Baltz et al., 2010; Gullo et al., 2010). Inhibition or disinhibition both cause BD to shorter. The former occurs with reduced IBSR whereas the second occurs with increased IBSR. Indicators of network bursting synchrony were differentially impacted by RF and MU. During the two forms of inhibition BD and IBSR synchrony decreased over the network but only MU shifted network bursting behavior from regular and synchronized to more irregular and less synchronized. This observation suggests that the effects of RF exert less constraints on network functioning than those mediated by the activation of $GABA_A$ receptor. The desynchronizing effect of MU on network bursting behavior can be most likely attributed to its hyperpolarizing action. Indeed, it has been shown that inverting the polarity of the GABA action, i.e. depolarizing toward hyperpolarizing, can evoke desynchronized premature-like network activity in young cultures moderately synchronized (Baltz et al., 2010).

Upon recovery from the inhibitory effects of MU but not from those of RF, networks showed a dramatic regain in bursting activity that persisted recurrently in a synchronous manner for ~1 min. This phenomenon relies most likely on the intrinsic property of cortical neurons so-called postinhibitory rebound and refers to the ability of a neuron to generate rebound excitation upon termination of an inhibitory signal (de la Peña and Geijo-Barrientos, 1996; Kawaguchi, 1993). Postinhibitory rebound is involved in a variety of basic brain processes such as rhythmic recurrent activity (Sanchez-Vives and McCormick, 2000) and short-term plasticity (Winograd et al., 2008). This phenomenon relies on several mechanisms occurring in response to hyperpolarization such as activation of hyperpolarization-activated cyclic nucleotide-gated (HCN) channels and deinactivation of low voltage-activated T-type calcium channels and persistent sodium channels (Boehme et al., 2011; Ferrante et al., 2017; Kurowski et al., 2018; Wu et al., 2005). In our conditions, postinhibitory rebound occurred in response to washout of MU and consecutive removal of tonic hyperpolarization. The absence of postinhibitory rebound in response to RF cessation might furthermore imply that RF exert their inhibitory effects without hyperpolarising neurons. Reduced bursting activity combined to the lack of postinhibitory rebound might suggest that RF fields potentially interferes with the functioning of ion channels involved in these modalities such as of HCN, T-type calcium channels and persistent sodium channels. Interestingly, it has been reported that exposure to extremely low-frequency-EMF (50 Hz, 0.2 mT, 1 hour) inhibited T-type calcium channels in mouse cortical neurons (Cui et al., 2014). However, no comparison with other types of currents were performed thus making difficult to test the relevance of this observation in the frame of the present study (see Pall, 2013; Wood and Karipidis, 2021, for reviews on EMF and calcium). Nevertheless, the rapid onset of the effects of RF-fields and their reversibility are in favour of a mechanism interacting with fast operating targets at the membrane such as ion channels. For a detailed review on EMF with cell membrane, organelles and biomolecules see Romanenko et al., (2017). Thorough investigations

with co-exposure of RF fields and pharmacological agents will enable to test directly potential interactions with ion channels.

Analysis of AP waveform showed that RF and MU-induced inhibition co-occurred with a slight symmetrical narrowing effect of the AP half-width. Although other studies reported on the narrowing effect of RF on AP waveform (Pikov et al., 2010; Romanenko et al., 2014; Wang et al., 2017, but see Wachtel et al., 1975; Razavinasab et al., 2016) the mechanism of action through which RF alter AP waveform remained to be established. Change in AP half-width exert direct influences on the efficiency of synaptic transmission (Sabatini and Regehr, 1997; Qian and Saggau, 1999; Kress and Mennerick, 2009; Ramezani and Akan, 2018) and might contribute to the inhibitory effect of RF on network bursting activity. Commonalities in the change in AP waveform in response to RF and MU suggest a potential overlapping mechanism between these two modalities. A possible point of convergence could be a similar effect on the membrane resistance. Indeed, decrease in membrane resistance in response to MU (Baufreton et al., 2001, Du and Bradley, 1998) was also observed in response to RF fields (Arber, 1981; Arber and Lin, 1985; but see Field et al., 1993; Ginsburg et al., 1992; Wachtel et al., 1975) and millimeter waves (MMWs, 30-300 GHz, Pikov et al., 2010). Shape of AP strongly relate to membrane resistance, with decreased and increased resistance being respectively associated to narrower and broader AP (Volgushev et al., 2000; Hedrick and Waters, 2011). Membrane resistance and AP waveform are also very sensitive to change in temperature with increased and decreased temperature leading respectively to lower/narrower and higher/broader membrane resistance and AP (Goldin and Mindin, 2017, Liu et al., 2021, Hedrick and Waters, 2011; Volgushev et al., 2000). Therefore, it cannot be excluded that the observed effect on AP waveform as a thermal origin (Romanenko et al., 2014). Recently, it was reported that midinfrared radiations also shorten AP by accelerating its repolarization, through an increase in voltage-gated potassium currents (Liu et al., 2021). Mechanisms of RF fields might differ from midinfrared radiation as

they manifest predominantly by a stepper depolarisation phase. Detailed electrophysiological experiments combined to accurate temperature control or bulk heating are required to disentangle the mechanism of RF on AP waveform. Moreover the hypothesis through which decreased AP half-width contributes to decrease network bursting behavior could be investigated in silico with neural simulation.

References

Apollonio F, Liberti M, Paffi A, Merla C, Marracino P, Denzi A, et al. Feasibility for Microwaves Energy to Affect Biological Systems Via Nonthermal Mechanisms: A Systematic Approach. IEEE Trans Microwave Theory Techn. 2013;61: 2031–2045. https://doi.org/10.1109/TMTT.2013.2250298

Arber SL, Lin JC. Microwave-induced changes in nerve cells: Effects of modulation and temperature. Bioelectromagnetics. 1985;6: 257–270. https://doi.org/10.1002/bem.2250060306

Arber SL. The Effect of Microwave Radiation on Passive Membrane Properties of Snail Neurons. Journal of Microwave Power. 1981;16: 15–20. https://doi.org/10.1080/16070658.1981.11689217

Arnold FJL, Hofmann F, Bengtson CP, Wittmann M, Vanhoutte P, Bading H. Microelectrode array recordings of cultured hippocampal networks reveal a simple model for transcription and protein synthesis-dependent plasticity: Transcription-dependent neuronal network plasticity. The Journal of Physiology. 2005;564: 3–19. https://doi.org/10.1113/jphysiol.2004.077446

Bader BM, Steder A, Klein AB, Frølund B, Schroeder OHU, Jensen AA. Functional characterization of GABAA receptor-mediated modulation of cortical neuron network activity in microelectrode array recordings. Cymbalyuk G, editor. PLoS ONE. 2017;12: e0186147. https://doi.org/10.1371/journal.pone.0186147

Baltz T, de Lima AD, Voigt T. Contribution of GABAergic interneurons to the development of spontaneous activity patterns in cultured neocortical networks. Front Cell Neurosci. 2010 Jun 21;4:15. https://doi.org/10.3389/fncel.2010.00015

Baufreton J, Garret M, Dovero S, Dufy B, Bioulac B, Taupignon A. Activation of GABA A Receptors in Subthalamic Neurons In Vitro: Properties of Native Receptors and Inhibition Mechanisms. Journal of Neurophysiology. 2001;86: 75–85. https://doi.org/10.1152/jn.2001.86.1.75

Belpomme D, Hardell L, Belyaev I, Burgio E, Carpenter DO. Thermal and non-thermal health effects of low intensity non-ionizing radiation: An international perspective. Environmental Pollution. 2018;242: 643–658. https://doi.org/10.1016/j.envpol.2018.07.019

Boehme R, Uebele VN, Renger JJ, Pedroarena C. Rebound excitation triggered by synaptic inhibition in cerebellar nuclear neurons is suppressed by selective T-type calcium channel block. Journal of Neurophysiology. 2011;106: 2653–2661. https://doi.org/10.1152/jn.00612.2011

Bologna LL, Pasquale V, Garofalo M, Gandolfo M, Baljon PL, Maccione A, et al. Investigating neuronal activity by SPYCODE multi-channel data analyzer. Neural Networks. 2010;23: 685–697. https://doi.org/10.1016/j.neunet.2010.05.002

Bolshakov MA, Alekseev SI. Bursting responses of Lymnea neurons to microwave radiation. Bioelectromagnetics. 1992;13: 119–129. https://doi.org/10.1002/bem.2250130206

Cain SM, Snutch TP. T-type calcium channels in burst-firing, network synchrony, and epilepsy. Biochimica et Biophysica Acta (BBA) - Biomembranes. 2013;1828: 1572–1578. https://doi.org/10.1016/j.bbamem.2012.07.028

Croft RJ, Hamblin DL, Spong J, Wood AW, McKenzie RJ, Stough C. The effect of mobile phone electromagnetic fields on the alpha rhythm of human electroencephalogram. Bioelectromagnetics. 2008;29: 1–10. https://doi.org/10.1002/bem.20352

Croft RJ, Leung S, McKenzie RJ, Loughran SP, Iskra S, Hamblin DL, Cooper NR. Effects of 2G and 3G mobile phones on human alpha rhythms: Resting EEG in adolescents, young adults, and the elderly. Bioelectromagnetics. 2010 Sep;31(6):434-44. https://doi.org/10.1002/bem.20583

Cui Y, Liu X, Yang T, Mei Y-A, Hu C. Exposure to extremely low-frequency electromagnetic fields inhibits T-type calcium channels via AA/LTE4 signaling pathway. Cell Calcium. 2014;55: 48–58. https://doi.org/10.1016/j.ceca.2013.11.002

de la Peña E, Geijo-Barrientos E. Laminar Localization, Morphology, and Physiological Properties of Pyramidal Neurons that Have the Low-Threshold Calcium Current in the Guinea-Pig Medial Frontal Cortex. J Neurosci. 1996;16: 5301–5311. https://doi.org/10.1523/JNEUROSCI.16-17-05301.1996

Du J, Bradley RM. Effects of GABA on acutely isolated neurons from the gustatory zone of the rat nucleus of the solitary tract. Chem Senses. 1998 Dec;23(6):683-8. https://doi.org/10.1093/chemse/23.6.683

Dunn SM, Thuynsma RP. Reconstitution of purified GABAA receptors: ligand binding and chloride transporting properties. Biochemistry. 1994 Jan 25;33(3):755-63. https://doi.org/10.1021/bi00169a017

El Khoueiry C, Moretti D, Renom R, Camera F, Orlacchio R, Garenne A, et al. Decreased spontaneous electrical activity in neuronal networks exposed to radiofrequency 1,800 MHz signals. Journal of Neurophysiology. 2018;120: 2719–2729. https://doi.org/10.1152/jn.00589.2017

Eulitz C, Ullsperger P, Freude G, Elbert T. Mobile phones modulate response patterns of human brain activity: NeuroReport. 1998;9: 3229–3232. https://doi.org/10.1097/00001756-199810050-00018

Fardet T, Ballandras M, Bottani S, Métens S, Monceau P. Understanding the Generation of Network Bursts by Adaptive Oscillatory Neurons. Front Neurosci. 2018;12: 41. https://doi.org/10.3389/fnins.2018.00041

Farrant M, Nusser Z. Variations on an inhibitory theme: phasic and tonic activation of GABAA receptors. Nat Rev Neurosci. 2005;6: 215–229. https://doi.org/10.1038/nrn1625

Ferrante M, Shay CF, Tsuno Y, William Chapman G, Hasselmo ME. Post-Inhibitory Rebound Spikes in Rat Medial Entorhinal Layer II/III Principal Cells: In Vivo, In Vitro, and Computational Modeling Characterization. Cereb Cortex. 2017 Mar 1;27(3):2111-2125. https://doi.org/10.1093/cercor/bhw058

Ferreri F, Curcio G, Pasqualetti P, De Gennaro L, Fini R, Rossini PM. Mobile phone emissions and human brain excitability. Ann Neurol. 2006;60: 188–196. https://doi.org/10.1002/ana.20906

Field AS, Ginsburg K, Lin JC. The effect of pulsed microwaves on passive electrical properties and interspike intervals of snail neurons. Bioelectromagnetics. 1993;14: 503–520. https://doi.org/10.1002/bem.2250140603

Foster KR, Glaser R. Thermal mechanisms of interaction of radiofrequency energy with biological systems with relevance to exposure guidelines. Health Physics. 2007;92: 609–620. https://doi.org/10.1097/01.HP.0000262572.64418.38

Foster KR. Thermal and nonthermal mechanisms of interaction of radio-frequency energy with biological systems. IEEE Trans Plasma Sci. 2000;28: 15–23. https://doi.org/10.1109/27.842819

Ginsburg KS, Lin JC, O'Neill WD. Microwave effects on input resistance and action potential firing of snail neurons. IEEE Trans Biomed Eng. 1992;39: 1011–1021. https://doi.org/10.1109/10.161333

Goldin MA, Mindlin GB. Temperature manipulation of neuronal dynamics in a forebrain motor control nucleus. Troyer TW, editor. PLoS Comput Biol. 2017;13: e1005699. https://doi.org/10.1371/journal.pcbi.1005699

Graves, S., Piepho, H.-S., and Selzer, L., with help Dorai-Raj, S., (2019). multcompView: Visualizations of Paired Comparisons. R package version 0.1-8. https://CRAN.R-project.org/package=multcompView

Greenebaum, B. & Barnes, F. Handbook of Biological Effects of Electromagnetic Fields, Vol. 1. Biological and Medical Aspects of Electromagnetic Fields 4th edn. (CRC Press, Boca Raton, 2019).

Gullo F, Mazzetti S, Maffezzoli A, Dossi E, Lecchi M, Amadeo A, Krajewski J, Wanke E. Orchestration of "presto" and "largo" synchrony in up-down activity of cortical networks. Front Neural Circuits. 2010 Apr 22;4:11. https://doi.org/10.3389/fncir.2010.00011

Hinrikus H, Bachmann M, Lass J. Understanding physical mechanism of low-level microwave radiation effect. International Journal of Radiation Biology. 2018;94: 877–882. https://doi.org/10.1080/09553002.2018.1478158

Hossmann K-A, Hermann DM. Effects of electromagnetic radiation of mobile phones on the central nervous system. Bioelectromagnetics. 2003;24: 49–62. https://doi.org/10.1002/bem.10068

ICNIRP (International Commission on Non-Ionizing Radiation Protection). Guidelines for Limiting Exposure to Electromagnetic Fields (100 kHz to 300 GHz). Health Phys. 2020 May;118(5):483-524. https://doi.org/10.1097/HP.0000000000001210

Kassambara A (2020). ggpubr: 'ggplot2' Based Publication Ready Plots. R package version 0.4.0. https://CRAN.R-project.org/package=ggpubr

Kawaguchi Y. Groupings of nonpyramidal and pyramidal cells with specific physiological and morphological characteristics in rat frontal cortex. Journal of Neurophysiology. 1993;69: 416–431. https://doi.org/10.1152/jn.1993.69.2.416

Kim JH, Lee J-K, Kim H-G, Kim K-B, Kim HR. Possible Effects of Radiofrequency Electromagnetic Field Exposure on Central Nerve System. Biomolecules & Therapeutics. 2019;27: 265–275. https://doi.org/10.4062/biomolther.2018.152

Kleinlogel H, Dierks Th, Koenig Th, Lehmann H, Minder A, Berz R. Effects of weak mobile phone-Electromagnetic fields (GSM, UMTS) on event related potentials and cognitive functions. Bioelectromagnetics. 2008;29: 488–497. https://doi.org/10.1002/bem.20418

Köhler T, Wölfel M, Ciba M, Bochtler U, Thielemann C. Terrestrial Trunked Radio (TETRA) exposure of neuronal in vitro networks. Environmental Research. 2018;162: 1–7. https://doi.org/10.1016/j.envres.2017.12.007

Kress GJ, Mennerick S. Action potential initiation and propagation: Upstream influences on neurotransmission. Neuroscience. 2009;158: 211–222. https://doi.org/10.1016/j.neuroscience.2008.03.021

Kurowski P, Grzelka K, Szulczyk P. Ionic Mechanism Underlying Rebound Depolarization in Medial Prefrontal Cortex Pyramidal Neurons. Front Cell Neurosci. 2018;12: 93. https://doi.org/10.3389/fncel.2018.00093

Linz KW, von Westphalen C, Streckert J, Hansen V, Meyer R. Membrane potential and currents of isolated heart muscle cells exposed to pulsed radio frequency fields. Bioelectromagnetics. 1999 Dec;20(8):497-511.https://doi.org/10.1002/(SICI)1521-186X(199912)20:8<497::AID-BEM4>3.0.CO;2-5

Liu X, Qiao Z, Chai Y, Zhu Z, Wu K, Ji W, et al. Nonthermal and reversible control of neuronal signaling and behavior by midinfrared stimulation. Proc Natl Acad Sci USA. 2021;118: e2015685118. https://doi.org/10.1073/pnas.2015685118

Maccione A, Gandolfo M, Massobrio P, Novellino A, Martinoia S, Chiappalone M. A novel algorithm for precise identification of spikes in extracellularly recorded neuronal signals. Journal of Neuroscience Methods. 2009;177: 241–249. https://doi.org/10.1016/j.jneumeth.2008.09.026

Mangiafico S. (2020). rcompanion: Functions to Support Extension Education Program Evaluation. R package version 2.3.25. https://CRAN.R-project.org/package=rcompanion

Marchionni I, Paffi A, Pellegrino M, Liberti M, Apollonio F, Abeti R, et al. Comparison between low-level 50 Hz and 900 MHz electromagnetic stimulation on single channel ionic currents and on firing frequency in dorsal root ganglion isolated neurons. Biochimica et Biophysica Acta (BBA) - Biomembranes. 2006;1758: 597–605. https://doi.org/10.1016/j.bbamem.2006.03.014

Merla C, Ticaud N, Arnaud-Cormos D, Veyret B, Leveque P. Real-Time RF Exposure Setup Based on a Multiple Electrode Array (MEA) for Electrophysiological Recording of Neuronal Networks. IEEE Trans Microwave Theory Techn. 2011;59: 755–762. https://doi.org/10.1109/TMTT.2010.2100404

Moretti D, Garenne A, Haro E, Poulletier de Gannes F, Lagroye I, Lévêque P, et al. In-vitro exposure of neuronal networks to the GSM-1800 signal: GSM-1800 Exposure of Neuronal Networks. Bioelectromagnetics. 2013;34: 571–578. https://doi.org/10.1002/bem.21805

Nefzi A, Orlacchio R, Carr L, Lemercier CE, Khoueiry CE, Lewis N, et al. Dosimetry of Microelectrodes Array Chips for Electrophysiological Studies Under Simultaneous Radio Frequency Exposures. IEEE Trans Microwave Theory Techn. 2022;70: 1871–1881. https://doi.org/10.1109/TMTT.2021.3136296

Novellino A, Scelfo B, Palosaari T, Price A, Sobanski T, Shafer TJ, et al. Development of Micro-Electrode Array Based Tests for Neurotoxicity: Assessment of Interlaboratory Reproducibility with Neuroactive Chemicals. Front Neuroeng. 2011;4. https://doi.org/10.3389/fneng.2011.00004

Olsen RW, Sieghart W. International Union of Pharmacology. LXX. Subtypes of γ-Aminobutyric Acid A Receptors: Classification on the Basis of Subunit Composition, Pharmacology, and Function. Update. Pharmacol Rev. 2008;60: 243–260. https://doi.org/10.1124/pr.108.00505

Oster S, Daus AW, Erbes C, Goldhammer M, Bochtler U, Thielemann C. Long-term electromagnetic exposure of developing neuronal networks: A flexible experimental setup: Exposure of Developing Neuronal Networks. Bioelectromagnetics. 2016;37: 264–278. https://doi.org/10.1002/bem.21974

Pall ML. Electromagnetic fields act via activation of voltage-gated calcium channels to produce beneficial or adverse effects. J Cell Mol Med. 2013;17: 958–965. https://doi.org/10.1111/jcmm.12088

Pasquale V, Martinoia S, Chiappalone M. A self-adapting approach for the detection of bursts and network bursts in neuronal cultures. J Comput Neurosci. 2010;29: 213–229. https://doi.org/10.1007/s10827-009-0175-1

Perez-Reyes E. Molecular Physiology of Low-Voltage-Activated T-type Calcium Channels. Physiological Reviews. 2003;83: 117–161. https://doi.org/10.1152/physrev.00018.2002

Piepho H-P. An Algorithm for a Letter-Based Representation of All-Pairwise Comparisons. Journal of Computational and Graphical Statistics. 2004;13: 456–466. https://doi.org/10.1198/1061860043515

Pikov V, Arakaki X, Harrington M, Fraser SE, Siegel PH. Modulation of neuronal activity and plasma membrane properties with low-power millimeter waves in organotypic cortical slices. J Neural Eng. 2010;7: 045003. https://doi.org/10.1088/1741-2560/7/4/045003

Pohlert T (2020). PMCMRplus: Calculate Pairwise Multiple Comparisons of Mean Rank Sums Extended. R package version 1.4.4. https://CRAN.R-project.org/package=PMCMRplus

Qian J, Saggau P. Modulation of Transmitter Release by Action Potential Duration at the Hippocampal CA3-CA1 Synapse. Journal of Neurophysiology. 1999;81: 288–298. https://doi.org/10.1152/jn.1999.81.1.288

R Core Team (2021). R: A language and environment for statistical computing. R Foundation for Statistical Computing, Vienna, Austria. https://www.R-project.org/

Ramezani H, Akan OB. Impacts of Spike Shape Variations on Synaptic Communication. IEEE Trans.on Nanobioscience. 2018;17: 260–271. https://doi.org/10.1109/TNB.2018.2838056

Razavinasab M, Moazzami K, Shabani M. Maternal mobile phone exposure alters intrinsic electrophysiological properties of CA1 pyramidal neurons in rat offspring. Toxicol Ind Health. 2016;32: 968–979. https://doi.org/10.1177/0748233714525497

Rijal SO, Gross GW. Dissociation constants for GABAA receptor antagonists determined with neuronal networks on microelectrode arrays. Journal of Neuroscience Methods. 2008;173: 183–192. https://doi.org/10.1016/j.jneumeth.2008.05.025

Romanenko S, Begley R, Harvey AR, Hool L, Wallace VP. The interaction between electromagnetic fields at megahertz, gigahertz and terahertz frequencies with cells, tissues and organisms: risks and potential. J R Soc Interface. 2017;14: 20170585. https://doi.org/10.1098/rsif.2017.0585

Romanenko S, Siegel PH, Wagenaar DA, Pikov V. Effects of millimeter wave irradiation and equivalent thermal heating on the activity of individual neurons in the leech ganglion. Journal of Neurophysiology. 2014;112: 2423–2431. https://doi.org/10.1152/jn.00357.2014

Rubinsky L, Raichman N, Baruchi I, Shein M, Lavee J, Frenk H, et al. Study of hypothermia on cultured neuronal networks using multi-electrode arrays. Journal of Neuroscience Methods. 2007;160: 288–293. https://doi.org/10.1016/j.jneumeth.2006.09.017

Sabatini BL, Regehr WG. Control of Neurotransmitter Release by Presynaptic Waveform at the Granule Cell to Purkinje Cell Synapse. J Neurosci. 1997;17: 3425–3435. https://doi.org/10.1523/JNEUROSCI.17-10-03425.1997

Saito A, Takahashi M, Jimbo Y, Nakasono S. Non-conductive and miniature fiber-optic imaging system for real-time detection of neuronal activity in time-varying electromagnetic fields. Biosensors and Bioelectronics. 2017;87: 786–793. https://doi.org/10.1016/j.bios.2016.09.024

Saito A, Takahashi M, Makino K, Suzuki Y, Jimbo Y, Nakasono S. Response of Cultured Neuronal Network Activity After High-Intensity Power Frequency Magnetic Field Exposure. Front Physiol. 2018;9: 189. https://doi.org/10.3389/fphys.2018.00189

Sallard E, Letourneur D, Legendre P. Electrophysiology of ionotropic GABA receptors. Cell Mol Life Sci. 2021;78: 5341–5370. https://doi.org/10.1007/s00018-021-03846-2

Sanchez-Vives MV, McCormick DA. Cellular and network mechanisms of rhythmic recurrent activity in neocortex. Nat Neurosci. 2000;3: 1027–1034. https://doi.org/10.1038/79848

SCENIHR (Scientific Committee on Emerging and Newly Identified Health Risks). Potential health effects of exposure to electromagnetic fields (EMF). European Commission 2015: 1–288, 2015. https://doi.org/10.2772/75635

Schmid MR, Loughran SP, Regel SJ, Murbach M, Bratic Grunauer A, Rusterholz T, et al. Sleep EEG alterations: effects of different pulse-modulated radio frequency electromagnetic fields: Different pulse-modulated RF EMF and sleep EEG. Journal of Sleep Research. 2012;21: 50–58. https://doi.org/10.1111/j.1365-2869.2011.00918.x

Soueid M, Kohler S, Carr L, Bardet SM, O'Connor RP, Leveque P, et al. Electromagnetic Analysis of an Aperture Modified TEM Cell Including an ITO Layer for Real-Time Observation of Biological Cells Exposed to Microwaves. PIER. 2014;149: 193–204. https://doi.org/10.2528/PIER14053108

Tattersall JEH, Scott IR, Wood SJ, Nettell JJ, Bevir MK, Wang Z, et al. Effects of low intensity radiofrequency electromagnetic fields on electrical activity in rat hippocampal slices. Brain Research. 2001;904: 43–53. https://doi.org/10.1016/S0006-8993(01)02434-9

Teppola H, Aćimović J, Linne M-L. Unique Features of Network Bursts Emerge From the Complex Interplay of Excitatory and Inhibitory Receptors in Rat Neocortical Networks. Front Cell Neurosci. 2019;13: 377. https://doi.org/10.3389/fncel.2019.00377

van Rongen E, Croft R, Juutilainen J, Lagroye I, Miyakoshi J, Saunders R, et al. Effects of Radiofrequency Electromagnetic Fields on the Human Nervous System. Journal of Toxicology and Environmental Health, Part B. 2009;12: 572–597. https://doi.org/10.1080/10937400903458940

van Pelt J, Wolters PS, Corner MA, Rutten WLC, Ramakers GJA. Long-Term Characterization of Firing Dynamics of Spontaneous Bursts in Cultured Neural Networks. IEEE Trans Biomed Eng. 2004;51: 2051–2062. https://doi.org/10.1109/TBME.2004.827936

Volgushev M, Vidyasagar TR, Chistiakova M, Yousef T, Eysel UT. Membrane properties and spike generation in rat visual cortical cells during reversible cooling. The Journal of Physiology. 2000;522: 59–76. https://doi.org/10.1111/j.1469-7793.2000.0059m.x

Volkow ND, Tomasi D, Wang GJ, Vaska P, Fowler JS, Telang F, Alexoff D, Logan J, Wong C. Effects of cell phone radiofrequency signal exposure on brain glucose metabolism. JAMA. 2011 Feb 23;305(8):808-13. https://doi.org/10.1001/jama.2011.186

Wachtel H, Seaman R, Joines W. Effects of low-intensity microwaves on isolated neurons. Ann NY Acad Sci. 1975;247: 46–62. https://doi.org/10.1111/j.1749-6632.1975.tb35982.x

Wagenaar D, Pine J, Potter S. An extremely rich repertoire of bursting patterns during the development of cortical cultures. BMC Neurosci. 2006;7: 11. https://doi.org/10.1186/1471-2202-7-11

Wang K, Lu J-M, Xing Z-H, Zhao Q-R, Hu L-Q, Xue L, et al. Effect of 1.8 GHz radiofrequency electromagnetic radiation on novel object associative recognition memory in mice. Sci Rep. 2017;7: 44521. https://doi.org/10.1038/srep44521

Wang Y-Y, Qin J, Han Y, Cai J, Xing G-G. Hyperthermia induces epileptiform discharges in cultured rat cortical neurons. Brain Research. 2011;1417: 87–102. https://doi.org/10.1016/j.brainres.2011.08.027

Hedrick T, Waters J. Spiking patterns of neocortical L5 pyramidal neurons in vitro change with temperature. Front Cell Neurosci. 2011 Jan 25;5:1. https://doi.org/10.3389/fncel.2011.00001

Winograd M, Destexhe A, Sanchez-Vives MV. Hyperpolarization-activated graded persistent activity in the prefrontal cortex. Proceedings of the National Academy of Sciences. 2008;105: 7298–7303. https://doi.org/10.1073/pnas.0800360105

Wood A, Karipidis K. Radiofrequency Fields and Calcium Movements Into and Out of Cells. Radiat Res. 2021 Jan 1;195(1):101-113. https://doi.org/10.1667/RADE-20-00101.1

Wu N, Hsiao C-F, Chandler SH. Membrane Resonance and Subthreshold Membrane Oscillations in Mesencephalic V Neurons: Participants in Burst Generation. J Neurosci. 2001;21: 3729–3739. https://doi.org/10.1523/JNEUROSCI.21-11-03729.2001

Xu S, Ning W, Xu Z, Zhou S, Chiang H, Luo J. Chronic exposure to GSM 1800-MHz microwaves reduces excitatory synaptic activity in cultured hippocampal neurons. Neuroscience Letters. 2006;398: 253–257. https://doi.org/10.1016/j.neulet.2006.01.004

Zwartsen A, Hondebrink L, de Lange DW, Westerink RHS. Hyperthermia exacerbates the acute effects of psychoactive substances on neuronal activity measured using microelectrode arrays (MEAs) in rat primary cortical cultures in vitro. Toxicology and Applied Pharmacology. 2020;397: 115015. https://doi.org/10.1016/j.taap.2020.115015

Supporting information

S1 Table. Metrics definition: Analysis of neural network activity

S2 Table. Raw values at baseline of the different metrics used to describe neural networks activity across the different experimental groups. Data expressed as Median (IQR). *(1) Indicates significant difference between SH-RF and SH-MU pairs ($p < 0.05$) and *(2) indicate significant difference between MU-SH and MU-RF pairs ($p < 0.05$), ^{ns} indicates no significant differences between groups. Pairwise comparison done with Kruskal-Wallis test followed by Conover's all-pairs posthoc test. SH, n = 12; RF, n = 15; MU, n = 8.

S1 Fig. AP detection, sorting, clusters repartition and waveform analysis. (A) From left to right: Mean AP detection for unsorted and sorted AP fraction (% of total detected AP); Relative fraction of sorted APs attributed to Major (MAJ), Auxiliary (AUX) and Minors (MIN) clusters; Mean AP count for sorted AP occurring either in (AP IB) or outside (AP OB) bursts period. Data collected over 15 min during pre-exposure phase from 15 cultures of the RF group used here as representative. (B) Example of sorted AP waveforms after principal component analysis and hierarchical classification, overlay of 125 waveforms per cluster with averaged waveform

highlighted, data from one channel of a same culture. Scale: (y): 40 µV; (x): 500 µs. (C) Illustration of the metrics used to quantify change in AP waveforms. FWHM: full width at half maximum. As recorded extracellularly the AP waveform is inverted. Scale: (y): 10 µV; (x): 500 µs.

S3 Table. Metrics definition: Analysis of AP waveform

S4 Table. Average raw values at baseline of the different metrics used to quantify change in AP waveform across the different experimental groups. Data expressed as Median (IQR). * Indicates significant difference ($p < 0.05$) between MU-SH and MU-RF pairs. Pairwise comparison done with Kruskal-Wallis test followed by Conover's all-pairs posthoc test. SH, n = 12; RF, n = 15; MU, n = 8.

Acknowledgments

The authors thanks Stephano Buccelli for its contribution in implementing new scripts in the software package SPYCODE. The authors thanks Patrik Krieger for sharing tools for spike sorting.

Author Contributions

Conceptualization: André Garenne, Isabelle Lagroye, Noëlle Lewis.

Data Curation: na.

Formal Analysis: Clément E. Lemercier.

Funding Acquisition: André Garenne, Delia Arnaud-Cormos, Philippe Levêque, Isabelle Lagroye, Noëlle Lewis.

Investigation : Clément E. Lemercier.

Methodology: na.

Project Administration: Noëlle Lewis.

Resources: Noëlle Lewis.

Software: na.

Supervision: André Garenne, Noëlle Lewis.

Validation: na.

Visualization: Clément E. Lemercier.

Writing – Original Draft Preparation: Clément E. Lemercier

Writing – Review & Editing: Clément E. Lemercier, André Garenne, Florence Poulletier de Gannes, Corinne El Khoueiry, Delia Arnaud-Cormos, Philippe Levêque, Isabelle Lagroye, Yann Percherancier, Noëlle Lewis.

Data Availability Statement

All relevant data are within the manuscript and its Supporting Information files.

Funding

This work was supported by the French National Research Program for Environmental and Occupational Health of Anses under Grant 2015/2 RF/19, by the European Union's Horizon 2020 Research and Innovation Program under Grant 737164 and by the Region Nouvelle-Aquitaine under Grant AAPR2020A-2019-8152210. The funders had no role in study design, data collection and analysis, decision to publish, or preparation of the manuscript

Competing interests

The authors have declared that no competing interests exist.

Supporting information

S1 Table. Metrics definition: Analysis of neural network activity

Analysis of neural network activity	
Metrics	
Day in vitro (DIV)	Age of the culture (in days) from preparation date (DIV_0) to recording date (DIV_n)
Active channel (k)	Number of channels showing both spiking and bursting activities
Mean spike rate (MSR)	Sum of channel mean spike rate (sec $^{-1}$)
Mean burst rate (MBR)	Sum of channel mean burst rate (sec $^{-1}$)
Network bursting rate (NtBR)	Rate of bursts occurring simultaneously in $\geq$ 20 channels (min $^{-1}$)
% of spike outside bursts	Ratio of the number of spikes outside bursts to the total of number of spikes.
Mean Interburst interval (IBI)	Pooled mean of mean channel IBI (sec)
Mean Burst duration (BD)	Pooled mean of mean channel BD (msec)
Mean intraburst spike rate (IBSR)	Pooled mean of mean channel IBSR (n spike in burst / burst duration)*1000), Hz)
Coefficient of variation (CV)	Ratio (expressed in %) of the average channels standard deviation to the metric mean value (either IBI, BD or IBSR)
Initial inhibitory rate	Linear regression of 4 points over peri-exposure period, 2 min before exposure-onset and 2 min after exposure-onset
Postinhibitory rebound	Ratio between the maximal values (either MBR or MSR) retrieved in two consecutive non-overlapping windows of 4 min after exposure-offset

S2 Table. Raw values at baseline of the different metrics used to describe neural networks activity across the different experimental groups.

Metrics	SH	RF	MU
N culture	12	15	8
N culture per animal	2 (3)	4 (3.5)	3 (1.5)
Day In Vitro	18.5 (1.5)	20 (2)	23 (2.5) *(2)
Active k	49 (13)	54 (6)	54 (5)
MSR (sec^{-1})	15.6 (18.5)	23.4 (37.3)	52 (43.2) *(2)
MBR (sec^{-1})	2.5 (2.6)	3.5 (2)	11.3 (12.7) *(2)
NtBR (min-1)	3.9 (5.3)	3.3 (1.6)	16.9 (16.4) *(2)
% of spike outside bursts	28.3 (21.9)	25 (21.5)	16.9 (12.3)
IBI (sec)	40.3 (35.6)	23.9 (11.8)	6.8 (10.5) *(2)
CV IBI (%)	19.3 (13.7)	17.4 (8.8)	8.8 (7.7) ns
BD (ms)	89 (102.5) *(1)	217 (91.8)	200.6 (115.4)
CV BD (%)	7 (3.4)	5.2 (3)	4.2 (1.8) *(2)
IBSR (Hz)	160.3 (46.9)	131.4 (42)	122 (35.9)
CV IBSR (%)	6.8 (3.9)	5.1 (2.1)	4.2 (2.3)

Data expressed as Median (IQR). *(1) Indicates significant difference between SH-RF and SH-MU pairs ($p < 0.05$) and *(2) indicate significant difference between MU-SH and MU-RF pairs ($p < 0.05$), ns indicates no significant differences between groups. Pairwise comparison done with Kruskal-Wallis test followed by Conover's all-pairs posthoc test. SH, n = 12; RF, n = 15; MU, n = 8.

S1 Fig. AP detection, sorting, clusters repartition and waveform analysis

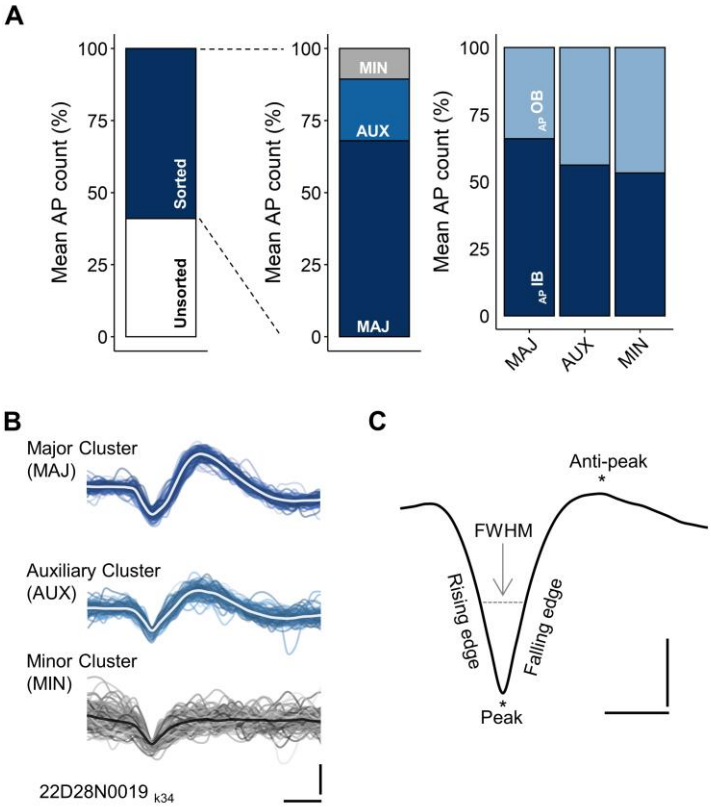

(A) From left to right: Mean AP detection for unsorted and sorted AP fraction (% of total detected AP); Relative fraction of sorted APs attributed to Major (MAJ), Auxiliary (AUX) and Minors (MIN) clusters; Mean AP count for sorted AP occurring either in ($_{AP}$ IB) or outside ($_{AP}$ OB) bursts period. Data collected over 15 min during pre-exposure phase from 15 cultures of the RF group used here as representative. (B) Example of sorted AP waveforms after principal component analysis and hierarchical classification, overlay of 125 waveforms per cluster with averaged waveform highlighted, data from one channel of a same culture. Scale: (y): 40 µV; (x): 500 µs. (C) Illustration of the metrics used to quantify change in AP waveforms. FWHM: full width at half maximum. As recorded extracellularly the AP waveform is inverted. Scale: (y): 10 µV; (x): 500 µs.

S3 Table. Metrics definition: Analysis of AP waveform

Analysis of spike waveform	
Metrics	
Peak amplitude (µV)	Maximal amplitude of the first peak (negative going)
Anti-peak amplitude (µV)	Maximal amplitude of the second peak (positive going)
Half-width (µs)	Full width at half maximum (FWHM) of the first peak computed with linear interpolation
Rising edge (µV/ 10^{-01} ms)	Maximal slope of the AP rising edge (negative going)
Falling edge (µV/ 10^{-01} ms)	Maximal slope of the AP falling edge (positive going)

S4 Table. Average raw values at baseline of the different metrics used to quantify change in AP waveform across the different experimental groups

Metrics	**SH**	**RF**	**MU**
Channel per MEA (count)	53 (12)	54 (6.5)	53 (2.3)
Sorted AP (count)	23 266 (18 327)	31 713 (17 353)	139 499 (87 694) *
Peak amplitude (µV)	-27.3 (11.1)	-28.9 (6.2)	-29.1 (5.7)
Anti-peak amplitude (µV)	11.2 (7.8)	13.1 (6.5)	15.3 (2)
Half-width (µs)	224.6 (39.7)	247.9 (29.8)	253.5 (52.3)
Rising edge (µV/ 10^{-01} ms)	-12.8 (5.7)	-13.7 (3)	-13.9 (4.8)
Falling edge (µV/ 10^{-01} ms)	12.8 (7.3)	14.6 (3.8)	15.21 (6)

Data expressed as Median (IQR). * Indicates significant difference ($p < 0.05$) between MU-SH and MU-RF pairs. Pairwise comparison done with Kruskal-Wallis test followed by Conover's all-pairs posthoc test. SH, n = 12; RF, n = 15; MU, n = 8.